Pattern Recognition 69 (2017) 141–149

Contents lists available at ScienceDirect

Pattern Recognition

journal homepage: www.elsevier.com/locate/patcog

Notes on shape based tools for treating the objects ellipticity issues

Joviša Žunić[a,*], Ramakrishna Kakarala[b], Mehmet Ali Aktaş[c]

[a] Mathematical Institute of Serbian Academy of Sciences and Arts, Belgrade, Serbia
[b] Nanyang Technological University, School of Computer Engineering, Singapore
[c] Toros University, Computer Science, Turkey

ARTICLE INFO

Article history:
Received 6 May 2016
Revised 8 April 2017
Accepted 10 April 2017
Available online 13 April 2017

Keywords:
Shape
Ellipticity measure
Shape invariants
Image processing
Computer vision
Pattern analysis

ABSTRACT

In this paper we put under the same umbrella several well known results and establish several new results related to the shape based tools which treat the objects ellipticity issues. We start with a derivation of an explicit and closed formula for the computation of the ellipticity measures, from an infinite family, introduced recently. The new formula enables a fast computation of such measures, since it does not require any optimizing procedure for the computation, as it was the case before. In addition, the established formula enables an easy theoretical manipulation. As a result, we have discovered new shape features, as they are: (i) *The average shape ellipticity measure*, which might be interpreted as an average value of the estimated similarities between the shape considered and all the ellipses whose axes length ratio belongs to a certain, predefined, interval; (ii) *The maximal shape ellipticity measure*, which might be understood as the maximal possible similarity estimate between a given shape and an ellipses.

Some of the other results obtained relate strongly to the well-known measures and methods broadly used in shape based object analysis tasks.

© 2017 Elsevier Ltd. All rights reserved.

1. Introduction

The shape is an object property which has a big discriminative capacity since it allows many numerical characterizations. One of common approaches is to observe certain shape descriptors/properties (e.g. convexity, elongation, compactness, sigmodaility, etc.) cognizable and distinct for a certain application, and then develop methods for their numerical evaluation. Such evaluation methods herein are called *shape measures*. There are many shape measures developed so far. Just to mention some of them: convexity [23], circularity[1] [17,22,33], linearity [9,26], tortuosity [10], but there are many more. As it can be seen, there are shape descriptors with multiple measures developed for their numerical evaluation. This is as expected since there is no shape measure performing well in all applications. The shape ellipticity, which is the main subject of this paper, also has multiple measures defined for its computation. Notice that by the shape ellipticity we mean the similarity of a given shape to the planar region bounded by an ellipse. It is worth pointing out that the object/shape ellipticity is a recurrent topic in research, due back to 1910 (see [27]) till the most recent days [16], and many more, e.g. [24,32], just to mention two of them. A lot of work has been dedicated to solve the appearing, ellipticity associated, problems. Here we mention [13,14,19,21], from the areas of the astronomy, astrophysics, nano-particles analysis, and traffic analysis.

Apart from the shape measures mentioned, there are generic shape measures which are targeted to satisfy some of desirable properties (e.g. the invariance with respect to a class of transformations), rather than to evaluate some of shape properties. Among them are: Fourier invariants [29], different kind of moment invariants [5,11,30,31], integral invariants [12], shape-illumination invariants [2], and so on. The power of generic shape invariants comes from the fact that the number of such invariants is not upper bounded. A drawback is that their behavior is not well explained and cannot be predicted.

There another approaches, as well, to the shape analysis problems. Here in we mention statistics based ones (the topic usually named the *statistical shape analysis*. An idea [4] was to learn the space of typical shapes, from examples of a class of shapes (i.e. training data). This can then be used to analyze new shapes, e.g. measure the probability the new shape is a member of the shape class, or transform the new shape by projecting it into the learnt shape space. A statistical appearance model, that uses a probabilistic correspondence (rather than one-to-one correspondences,

* Corresponding author.
E-mail addresses: jovisa_zunic@mi.sanu.ac.rs (J. Žunić), Ramakrishna@ntu.edu.sg (R. Kakarala), mehmet.aktas@toros.edu.tr (M. Ali Aktaş).

[1] The circularity property is often called *compactness*, since the circular disc is understood as the most compact shape.

http://dx.doi.org/10.1016/j.patcog.2017.04.009
0031-3203/© 2017 Elsevier Ltd. All rights reserved.

for example) has been considered in [15]. A learning statistical shape model from image data, has been proposed in [8]. The model uses Kendal shape space, represents shapes as point set equivalence classes, and treats each shape point set as a random variable. A method for constructing statistical representations of ensembles of similar shapes is described in [3]. The method is based on an optimal distribution of a large set of surface point correspondences (the method uses surface point samples rather than any specific surface parameterization). Current (a generalized distribution, coming from geometric measure theory) based method for computing an optimal deformation between surfaces embedded in 3D space is given in [28]. The method leads to a diffeomorphic matching algorithm, with an immediate application in statistical inference of shapes, via momentum representation of flow.

As it could be expected, the measures which do relate to certain shape property have a well understood and predictable behavior, but their number is limited. This further causes a limited discriminative power of such measures. An attempt to balance between these two issues has been made in [1], where a tuning parameter $\rho \in (0, 1]$ was involved to design an infinite family of ellipticity measures $\mathcal{E}_\rho(S)$. All measures, from the family $\mathcal{E}_\rho(S)$, with $0 < \rho \leq 1$, are invariant with respect to translation, rotation, and scaling transformations and range over the interval (0, 1]. For a fixed $\rho \in (0, 1]$, the equality $\mathcal{E}_\rho(S) = 1$ is true if and only if the shape S is the ellipse whose the axes length ratio is ρ. Thus, the ellipticity measures $\mathcal{E}_\rho(S)$ distinguish between ellipses whose axes length ratios are different – i.e. such ellipses are considered to be different in shape, as well.

The results of [1] are actually the starting point for the work of this paper. We start with the derivation of an explicit and closed formula for $\mathcal{E}_\rho(S)$.[2] This enables a fast computation and more detailed theoretical observation of the properties of the measures from the family. Based on these observations we discover new shape measures/features, not discussed before in the literature:

- *Average ellipticity*, $\mathcal{E}_{avg}(S)$, is defined as the average score of the measured ellipticities $\mathcal{E}_\rho(S)$, while ρ varies through an interval $(a, b]$, with $0 < a < b \leq 1$.
- *Maximum ellipticity*, $\mathcal{E}_{\max}(S)$, is defined as the maximal value among all the ellipticity measures $\mathcal{E}_\rho(S)$, with $0 < \rho \leq 1$. Formally: $\mathcal{E}_{\max}(S) = \max_{\rho \in (0,1]} \mathcal{E}_\rho(S)$.[3]

Some of the obtained results strongly relate to the well-known results that are already in common use in image processing and computer vision tasks. This will be discussed in more details later on. Several illustrative examples are provided, in order to support a better understanding of the theoretical observations made in this paper.

The paper is organized as it follows: Section 2 gives the basic definitions and denotations. Explicit formulas for the computation of the $\mathcal{E}_\rho(S)$, $\mathcal{E}_{avg}(S)$, and $\mathcal{E}_{\max}(S)$, measures and related comments are Section 3. Concluding remarks are in Section 4.

2. Definitions and denotation

We list shortly the basic terms and denotations, used in the rest of the paper.

- $E(a, b)$ denotes an isothetic ellipse whose axis lengths are a and b, and whose centroid coincides with the origin. Formally,

$$E(a,b) = \left\{ (x,y) \mid \frac{x^2}{a^2} + \frac{y^2}{b^2} \leq 1 \right\}. \tag{1}$$

Just as a short reminder, the area of $E(a, b)$ is $\pi \cdot a \cdot b$.

Remark. Instead of the term 'ellipse', in mathematics assumed to be a line (not a region, as in (1)), more correct would be to use the term 'elliptical disc', for the region $E(a, b)$ in (1). However, we will proceed to use the term 'ellipse' because it has been commonly used in literature related to the shape analysis. Similarly, we will use the term 'circle' for planar region bounded by the circular line, instead of, mathematically more correct, term 'circular disc'.

- Since the shape does not change under scaling transformations, without loss of generality, we will assume that all appearing shapes have the area equal to 1.
- $E(\rho)$ will denote an isothetic ellipse, having the unit area and the axes length ratio equal to ρ, and placed such that the centroid of $E(\rho)$ coincides with the origin - i.e.

$$E(\rho) = \left\{ (x,y) \mid \frac{x^2}{\left(\sqrt{\frac{\rho}{\pi}}\right)^2} + \frac{y^2}{\left(\frac{1}{\sqrt{\pi \cdot \rho}}\right)^2} \leq 1 \right\} = \left\{ (x,y) \mid \frac{x^2}{\rho} + \rho \cdot y^2 \leq \frac{1}{\pi} \right\}. \tag{2}$$

In other words $E(\rho) = E(a, b)$, with $a = \sqrt{\rho/\pi}$ and $b = 1/\sqrt{\pi \cdot \rho}$.

- Two shapes are said to be equal if their set differences have the area equal to zero. This is not a restriction in practical applications – e.g. a closed region $\{(x, y) \mid x^2 + y^2 \leq 1\}$ and the open one $\{(x, y) \mid x^2 + y^2 < 1\}$ are of the same shape.
- $S(\omega)$ will denote the shape S rotated around its centroid for an angle ω. Notice that the shape centroid (x_c, y_c), as usually, is defined as

$$(x_c, y_c) = \left(\frac{\iint_S x \, dx \, dy}{\iint_S dx \, dy}, \frac{\iint_S y \, dx \, dy}{\iint_S dx \, dy} \right). \tag{3}$$

- The first two Hu moment invariants [11] will be used intensively in our derivations. They will be denoted by $\mathcal{H}_1(S)$ and $\mathcal{H}_2(S)$ respectively, and are defined as:

$$\mathcal{H}_1(S) = m_{2,0}(S) + m_{0,2}(S) \quad \text{and}$$
$$\mathcal{H}_2(S) = (m_{2,0}(S) - m_{0,2}(S))^2 + 4m_{1,1}(S)^2. \tag{4}$$

The quantities $m_{p,q}(S)$ are so called normalized moments and are defined as

$$m_{p,q}(S) = \iint_S (x - x_c)^p (y - y_c)^q \, dx \, dy, \tag{5}$$

for the shapes having the area equal to 1.

3. Family of ellipticity measures, maximal, and average ellipticity

A family of ellipticity measures $\mathcal{E}_\rho(S)$, dependent on a parameter $\rho \in (0, 1]$, has been introduced recently in [1]. The quantity $\mathcal{E}_\rho(S)$ evaluates the similarity between the considered shape S and the ellipse $E(\rho)$ (whose axes length ratio is ρ - see (2)), and is invariant w.r.t. translation, rotation and scaling transformations. Also, $\mathcal{E}_\rho(S) = 1$ if and only if $S = E(\rho)$.

The ellipticity measures $\mathcal{E}_\rho(S)$ are shown to be very efficient in a galaxy classification task [1]. The elliptical and spiral galaxies listed in the *Nearby Galaxy Catalog* (**NGC**) [7], were used as the data set (see Fig. 1 for some examples). This classification problem is a difficult task. Previous the best accuracy was 95.1% [18]. The 100% classification rate was achieved by employing a number of $\mathcal{E}_\rho(S)$ measures. A simple k-NN classifier was used. In addition, to reduce limits (in the classification efficiency), caused by a choice of the threshold method selected, two shapes were associated to

[2] The formula for the computation of $\mathcal{E}_\rho(S)$, derived in [1], involves an optimizing procedure and is suitable for the numerical computation only.

[3] It may be interesting to point out that $\mathcal{E}_{\max}(S)$ is invariant with respect to affine transformations, while the measures from the family $\mathcal{E}_\rho(S)$ are not.

Fig. 1. The first three images: The original image of an elliptical galaxy and its corresponding shapes after the global and local thresholding. The last three images: The original image of a spiral galaxy and its corresponding shapes after the global and local thresholding.

every galaxy. These two shapes are obtained by using both 'global' and 'local' version of the Otsu thresholding method [20] (see examples in Fig. 1). An average classification rate of 95.6%, based on 100 mutually independent experiments, was obtained as well. This is also better than the previous bench mark result of 95.1%. The classification rates obtained illustrate a high discriminative power of the ellipticity measures from the family $\mathcal{E}_\rho(S)$ and give arguments for a further investigation on their properties. To perform such an investigation, the initial expression for $\mathcal{E}_\rho(S)$, as given in Definition 1, from [1], should be simplified and given in a more suitable form.

Definition 1. Let a shape S, having the area equal to 1 and centroid coincident with the origin, be given. Let ρ be a number from the interval (0, 1] and $S(\omega)$ be the shape S rotated around the origin for an angle ω. The ellipticity measure $\mathcal{E}_\rho(S)$ is defined as

$$\mathcal{E}_\rho(S) = \frac{1}{2\cdot\pi}\cdot\frac{1}{\min\limits_{\omega\in[0,2\pi]}\iint_{S(\omega)}\left(\frac{x^2}{\rho}+\rho\cdot y^2\right)dx\,dy}. \tag{6}$$

The quantity in (6) allows an easy and straightforward numerical computation of $\mathcal{E}_\rho(S)$ values, but such a computation can be time consuming - depending on the image size and on the precision required. An additional problem is that the expression of $\mathcal{E}_\rho(S)$, as given in (6), is not suitable for a further manipulation and analysis. We will make an additional step forward in this paper – we derive an explicit and closed formula for the computation of $\mathcal{E}_\rho(S)$. After that, we will exploit this formula in further derivations. First, we give an auxiliary lemma (for a proof see the Appendix), which gives an explicit formula for the computation of the minimum appearing in (6).

Lemma 1. *Let a shape S whose area is 1 and whose centroid coincides with the origin, be given. Also, let $S(\omega)$ be the shape S rotated around the origin for an angle ω. The following equality is true:*

$$\min_{\omega\in[0,2\pi]}\left\{\iint_{S(\omega)}\left(\frac{x^2}{\rho}+\rho\cdot y^2\right)dx\,dy\right\} = \frac{\rho^2+1}{2\cdot\rho}\cdot\mathcal{H}_1(S)-\frac{1-\rho^2}{2\cdot\rho}\cdot\sqrt{\mathcal{H}_2(S)}. \tag{7}$$

Now we are able to give an explicit and closed formula for the computation of $\mathcal{E}_\rho(S)$.

Lemma 2. *Let a shape S whose area is 1 and whose centroid coincides with the origin, be given. The following formula is true for all $\rho \in (0, 1]$*

$$\mathcal{E}_\rho(S) = \frac{1}{\pi}\cdot\frac{\rho}{(1+\rho^2)\cdot\mathcal{H}_1(S)+(\rho^2-1)\cdot\sqrt{\mathcal{H}_2(S)}}. \tag{8}$$

Proof. The statement is a direct consequence of (6) and (7). □

Next, we give two statements (given below as corollaries) which follow easily from (8), but were not visible from (6), used previously for the computation of $\mathcal{E}_\rho(S)$. The first corollary says that the circularity measure $\mathcal{C}(S)$, introduced in [33], is a particular case of the $\mathcal{E}_\rho(S)$ measures. Indeed, if we set $\rho = 1$ then the ellipse $E(\rho)$ becomes a circle, and consequently the quantity $\mathcal{E}_{\rho=1}(S)$ evaluates how much the shape S differs from a circle $E(\rho = 1)$. It turns out that $\mathcal{E}_{\rho=1}(S) = \mathcal{C}(S)$. Thus, we have obtained the following corollary.

Corollary 1. *Let a shape S whose area is 1 and whose centroid coincides with the origin, be given. The measure $\mathcal{E}_{\rho=1}(S)$ coincides with the circularity measure $\mathcal{C}(S)$ from [33], i.e.*

$$\mathcal{E}_{\rho=1}(S) = \frac{1}{2\cdot\pi\cdot\mathcal{H}_1(S)} = \mathcal{C}(S). \tag{9}$$

The next corollary confirms a natural expectation that in the limit case, when $\rho \to 0$, the ellipticity $\mathcal{E}_\rho(S)$ also converges to 0, for every fixed shape S. In other words, none of fixed shapes is similar to an 'infinitely' elongated ellipse.

Corollary 2. *Let a shape S whose area is 1 and whose centroid coincides with the origin, be given. The following statement is true*

$$\lim_{\rho\to 0}\mathcal{E}_\rho(S) = \frac{1}{\pi}\cdot\lim_{\rho\to 0}\frac{\rho}{(1+\rho^2)\cdot\mathcal{H}_1(S)+(\rho^2-1)\cdot\sqrt{\mathcal{H}_2(S)}} = 0. \tag{10}$$

Proof. If $\mathcal{H}_1(S) > \sqrt{\mathcal{H}_2(S)}$ is provided then the statement in (10) follows easily. But $\mathcal{H}_1(S) > \sqrt{\mathcal{H}_2(S)}$ is always true. We will show this by showing that the statement $\mathcal{H}_1(S) \le \sqrt{\mathcal{H}_2(S)}$ leads to a contradiction. Indeed,

$$\mathcal{H}_1(S)^2 \le \mathcal{H}_2(S) \tag{11}$$

$$\Leftrightarrow\quad (m_{2,0}(S)+m_{0,2}(S))^2 \le (m_{2,0}(S)-m_{0,2}(S))^2+4\cdot m_{1,1}(S)^2 \tag{12}$$

$$\Leftrightarrow\quad m_{2,0}(S)\cdot m_{0,2}(S)-m_{1,1}(S)^2 \le 0 \tag{13}$$

$$\Leftrightarrow\quad \int_{(x,y)\in S}\int_{(u,v)\in S}\int(v\cdot v-u\cdot y)^2\,dx\,dy\,du\,dv \le 0. \tag{14}$$

The quantity on the left side of the inequality in (14) is strictly positive[4] for all the shapes S having non-zero area. So, the contradiction in (14) establishes the proof. □

Experimental Illustrations of $\mathcal{E}_\rho(S)$ Behavior. We give several examples to illustrate the theoretical observations above. More experiments, can be found in [1]. Based on the explicit and closed formula (8), derived here, it is easy to produce the graphs $\mathcal{E}_\rho(S)$, for $\rho \in (0, 1]$. Five randomly chosen shapes and their corresponding $\mathcal{E}_\rho(S)$ graphs are in Fig. 2. The graphs displayed illustrate several properties of $\mathcal{E}_\rho(S)$ measures. The shape in column (a) is pretty much circular and, because of that, the highest ellipticiy $\mathcal{E}_\rho(S)$ is for a ρ value close to 1. The fish shape in column (b) is comparable with an elongated ellipse. So, $\mathcal{E}_\rho(S)$ picks its maximum

[4] The equality: $m_{2,0}(S)\cdot m_{0,2}(S)-m_{1,1}(S)^2 = \int_{(x,y)\in S}\iint_{(u,v)\in S}\int(v\cdot v-u\cdot y)^2\,dx\,dy\,du\,dv$ comes from [31].

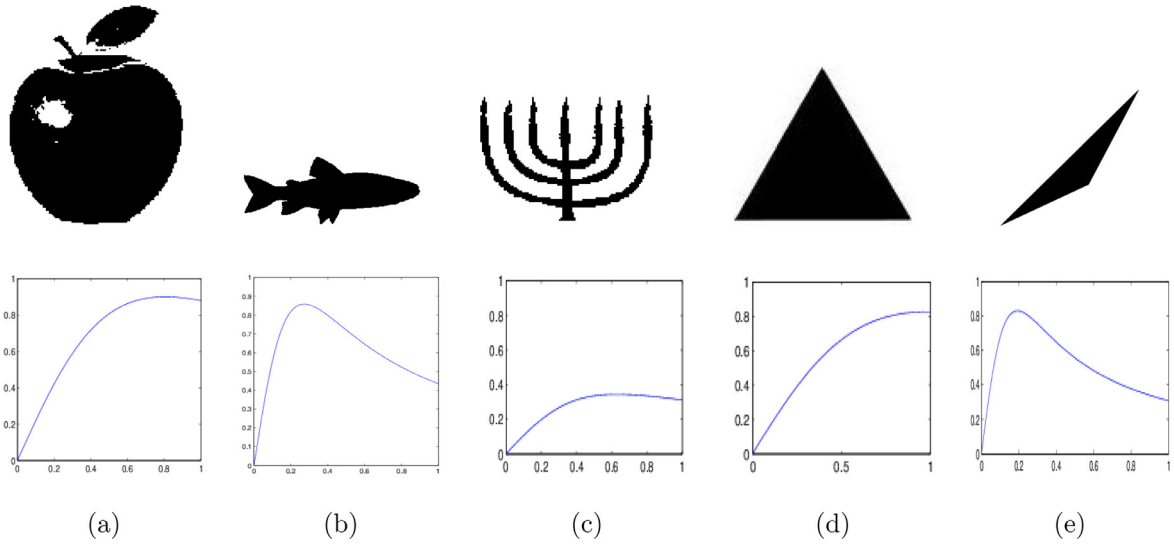

Fig. 2. Randomly selected shapes and their corresponding graphs $\mathcal{E}_\rho(S)$, for $\rho \in (0, 1]$.

for the ρ value not close to 1. The menora shape in column (c) cannot be understand as elliptical one (i.e. not similar to any ellipse) and this causes that the values of $\mathcal{E}_\rho(S)$ are never relatively close to 1. It is worth noticing the following: The maximal $\mathcal{E}_\rho(S)$ values, for the triangles displayed in the columns (d) and in (e), are the same (both equal to 0.8279) although reached for different values of the parameter ρ (see the graphs below the shapes). This is in accordance with the results presented in the next subsection.

Now, we give a two general remarks: **(i)**–From the graphs of $\mathcal{E}_\rho(S)$, for the shapes in (d) and (e), is easily visible that the measures $\mathcal{E}_\rho(S)$ are not affine invariant. Indeed, since any two triangles are affine invariant, the graphs of $\mathcal{E}_\rho(S)$ should be the same for all the triangles, but this is not the case. **(ii)**–As ρ approaches to 0, the $\mathcal{E}_\rho(S)$, values approach to 0, as well, for all the five shapes displayed. This is in accordance with Corollary 2.

3.1. Maximal ellipticity $\mathcal{E}_\rho(S)$ - for a fixed S

As it has been mentioned, $\mathcal{E}_\rho(S)$ takes strictly positive values (for any shape S and any $\rho \in (0, 1]$), while Corollary 2 says that $\mathcal{E}_\rho(S)$ approaches to 0 as $\rho \to 0$. A consequence is that there is no a parameter ρ_0 such that $\mathcal{E}_{\rho_0}(S) = \min\{\mathcal{E}_\rho(S) \mid \rho \in (0, 1]\}$, for a given shape S. In other words, there is no such an ellipse $E(\rho)$ which has the lowest similarity to a given shape S, measured by the ellipticity measures from the family $\mathcal{E}_\rho(S)$.

But the answer to the opposite question: *Does the ellipse $E(\rho)$ which is most similar to a given shape S, measured by the ellipticity measures from the family $\mathcal{E}_\rho(S)$, exist?* is positive. In this section we will show that, for any fixed shape, such an optimizing ellipse $E(\rho)$ is determined uniquely, and will give explicit formulas for: **(i)** The computation of the corresponding parameter ρ; and **(ii)** the computation of the reached maximum ellipticity $\mathcal{E}_{\max}(S) = \max_{\rho\in(0,1]} \mathcal{E}_\rho(S)$. It will turn out that such an optimal ellipse $E(\rho)$ correlates with the ellipse used commonly in the literature as a fitting ellipse to the given set of points.

Lemma 3. *Let a shape S be given. The largest ellipticity measure $\mathcal{E}_\rho(S)$, while ρ varies through* (0, 1], *can be computed as*

$$\mathcal{E}_{max}(S) = \max_{\rho\in(0,1]} \mathcal{E}_\rho(S) = \frac{1}{2 \cdot \pi \cdot \sqrt{\mathcal{H}_1(S)^2 - \mathcal{H}_2(S)}}. \tag{15}$$

Such a maximal ellipticity measure, $\max_{\rho\in(0,1]} \mathcal{E}_\rho(S)$, is reached for

$$\rho = \sqrt{\frac{\mathcal{H}_1(S) - \sqrt{\mathcal{H}_2(S)}}{\mathcal{H}_1(S) + \sqrt{\mathcal{H}_2(S)}}}. \tag{16}$$

Proof. The first derivative $d\mathcal{E}_\rho(S)/d\rho$, e.g. obtained from (8), is

$$\frac{d\mathcal{E}_\rho(S)}{d\rho} = \frac{-\rho^2 \cdot \left(\mathcal{H}_1(S) + \sqrt{\mathcal{H}_2(S)}\right) + \mathcal{H}_1(S) - \sqrt{\mathcal{H}_2(S)}}{\left((1+\rho^2) \cdot \mathcal{H}_1(S) + (\rho^2 - 1) \cdot \sqrt{\mathcal{H}_2(S)}\right)^2}. \tag{17}$$

Because of $\rho > 0$, $d\mathcal{E}_\rho(S)/d\rho$ vanishes if and only if ρ takes the value as given in (16). Since $\mathcal{E}_\rho(S) > 0$ and $\lim_{\rho\to 0} \mathcal{E}_\rho(S) = 0$, this is the point where $\mathcal{E}_\rho(S)$ reaches the maximum. Notice that $\mathcal{H}_1(S) > \sqrt{\mathcal{H}_2(S)}$ (see the proof of Corollary 2) implies that ρ, as given in (16), is well defined. For the shapes with $\mathcal{H}_2(S) = 0$ the maximum is reached for $\rho = 1$.

To prove (15), it is enough to enter (16) into the formula in (8). □

Examples Illustrating $\mathcal{E}_{\max}(S)$ Behavior. The results coming out from this analysis are not quite expected and might be referred as surprising ones. Indeed, in turns out that an affine invariant measure ($\mathcal{E}_{\max}(S)$) has been derived based on the family of the measures ($\mathcal{E}_\rho(S)$) which are not affine invariant. Notice that the relationship between $\mathcal{P}(S)$ and $\mathcal{E}_{\max}(S)$, established in (29), shows that $\mathcal{E}_{\max}(S)$ is also an affine invariant. Now, we give some examples (see Fig. 3) to illustrate the theoretical considerations given in this subsection.

The first shape, in Fig. 3, is pretty much circular. So, it is expected that the largest ellipticity will be computed if the shape is compared with an ellipse $E(\rho)$ whose axes length ratio ρ is close to 1. This is exactly what has happened, the largest ellipticity $\mathcal{E}_{\rho=0.8819}(S) = 0.8269$ is obtained for $\rho = 0.8819$. The maximal ellipticities for the next two shapes are 0.5922 and 0.5906, respectively. The small difference among them is caused by the numerical computation. Since $\mathcal{E}_{\max}(S)$ is an affine invariant and since those two shapes are affine invariant, the same maximal ellipticities are expected, independently on the value of ρ for which they are reached (in this case $\rho = 0.9363$ and $\rho = 0.2327$, respectively). The forth (fish) shape in fits well with the ellipse $E(\rho = 0.1359)$ and this explains a very high maximum ellipticity of 0.8280. Finally, the thin ring shape fits best with a circle (i.e. $\rho = 1$; the

$\max_{\rho\in(0,1]} \mathcal{E}_\rho(S)$: 0.8269 ($\rho = 0.8819$) 0.5922 ($\rho = 0.9363$) 0.5906 ($\rho = 0.2327$) 0.8280 ($\rho = 0.1359$) 0.0756 ($\rho = 0.9996$)

Fig. 3. Top row: randomly selected shapes; Second row: maximal ellipticities $\max_{\rho\in(0,1]} \mathcal{E}_\rho(S)$; Third row: parameter ρ values which corresponds to the maximal ellipticity.

disparency with the computed value $\rho = 0.9996$ is caused by the numerical computation). The computed maximal ellipticity is very low (equal to 0.0756), which is in accordance with our perception that there is no ellipse similar to such a thin ring.

3.2. The average ellipticity

In the literature, so far, an ellipticity measure was a single number used to express the degree to which a shape looks like an ellipse - either an arbitrary ellipse or a particular one (both approaches were utilized). Now, we are in position to define the quantity which averages all the ellipticity measures $\mathcal{E}_\rho(S)$, $\rho \in (0, 1]$, of a given set S. The following derivation:

$$\int_0^1 \mathcal{E}_\rho(S)d\rho = \frac{1}{\pi}\cdot\int_0^1 \frac{\rho}{(1+\rho^2)\cdot\mathcal{H}_1(S)+(\rho^2-1)\cdot\sqrt{\mathcal{H}_2(S)}}\,d\rho \tag{18}$$

$$= \frac{1}{2\cdot\pi\cdot(\mathcal{H}_1(S)+\sqrt{\mathcal{H}_2(S)})} \cdot \ln\left[(1+\rho^2)\cdot\mathcal{H}_1(S)+(\rho^2-1)\cdot\sqrt{\mathcal{H}_2(S)}\right]\Big|_{\rho\to 0}^{\rho=1} \tag{19}$$

$$= \frac{1}{2\cdot\pi\cdot\left(\mathcal{H}_1(S)+\sqrt{\mathcal{H}_2(S)}\right)}\cdot\ln\frac{2\cdot\mathcal{H}_1(S)}{\mathcal{H}_1(S)-\sqrt{\mathcal{H}_2(S)}}. \tag{20}$$

gives arguments and motivation for the next definition of a new shape measure - herein named the *average ellipticity*, and denoted as $\mathcal{E}_{avg}(S)$.

Definition 2. Let a shape S whose area is 1 and whose centroid coincides with the origin, be given. The average ellipticity of S is defined as

$$\mathcal{E}_{avg}(S) = \frac{1}{2\cdot\pi\cdot(\mathcal{H}_1(S)+\sqrt{\mathcal{H}_2(S)})}\cdot\ln\frac{2\cdot\mathcal{H}_1(S)}{\mathcal{H}_1(S)-\sqrt{\mathcal{H}_2(S)}}. \tag{21}$$

The average ellipticity measure $\mathcal{E}_{avg}(S)$, as given in (21), is the average value of all the ellipticity measures $\mathcal{E}_\rho(S)$, which evaluate the similarity between the shape S and all the ellipses $E(\rho)$ individually, while ρ varies through (0, 1]. If we replace the interval (0, 1] with a certain subinterval $(a, b]\subset(0, 1]$, and compute again the average value of the ellipticity measures $\mathcal{E}_\rho(S)$, but now varying the parameter ρ through the interval $(a, b]$, we obtain:

$$\frac{1}{b-a}\cdot\int_a^b \mathcal{E}_\rho(S)d\rho = \frac{1}{\pi\cdot(b-a)}\cdot\int_a^b \frac{\rho}{(1+\rho^2)\cdot\mathcal{H}_1(S)+(\rho^2-1)\cdot\sqrt{\mathcal{H}_2(S)}}\,d\rho \tag{22}$$

$$= \frac{1}{2\cdot\pi\cdot(b-a)\cdot(\mathcal{H}_1(S)+\sqrt{\mathcal{H}_2(S)})} \cdot \ln\frac{(1+b^2)\cdot\mathcal{H}_1(S)+(b^2-1)\cdot\sqrt{\mathcal{H}_2(S)}}{(1+a^2)\cdot\mathcal{H}_1(S)+(a^2-1)\cdot\sqrt{\mathcal{H}_2(S)}}. \tag{23}$$

In other words, we have derived the average ellipticity value, which results from the comparison of a given shape S with all the ellipses $E(\rho)$ whose axes length ratio ρ varies through $(a, b]\subset(0, 1]$. Thus, the following definition of the average ellipticity, $\mathcal{E}_{(a,b]}(S)$, related to a specific, (predefined) interval, comes naturally.

Definition 3. Let a shape S whose area is 1 and whose centroid coincides with the origin, be given. Fix the interval $(a, b]\subset(0, 1]$. The average ellipticity $\mathcal{E}_{(a,b]}(S)$, of S, is defined as

$$\mathcal{E}_{(a,b]}(S) = \frac{1}{2\pi(b-a)\left(\mathcal{H}_1(S)+\sqrt{\mathcal{H}_2(S)}\right)} \cdot \ln\frac{(1+b^2)\cdot\mathcal{H}_1(S)+(b^2-1)\cdot\sqrt{\mathcal{H}_2(S)}}{(1+a^2)\cdot\mathcal{H}_1(S)+(a^2-1)\cdot\sqrt{\mathcal{H}_2(S)}}. \tag{24}$$

It is worth mentioning that $\mathcal{E}_{avg}(S)$ and $\mathcal{E}_{(a,b]}(S)$ (for any choice of $a, b \in (0, 1]$) are invariant with respect to translation, rotation, and scaling transformations. This comes from their definition and also from the $\mathcal{E}_\rho(S)$ properties. We proceed with several examples to support a better understanding how $\mathcal{E}_{avg}(S)$ and $\mathcal{E}_{(a,b]}(S)$ act in the shape domain.

Examples Illustrating Average Shape Ellipticity Measures Behavior. The following examples illustrate the behavior of the shape measures $\mathcal{E}_{avg}(S)$ and $\mathcal{E}_{(0,d]}(S)$, with $d \in (0, 1]$. Five shapes are displayed in Fig. 4. The same shapes as in Fig. 3 are used, for an easier comparison with the behavior of $\mathcal{E}_{\max}(S)$. The corresponding average ellipticities $\mathcal{E}_{avg}(S)$ are in the second row. It is worth noticing that $\mathcal{E}_{avg}(S)$ is not an affine invariant, as it can be seen easily from the second and third shape. There is an affine transformation which maps the second shape into the third one, but their ellipticity $\mathcal{E}_{avg}(S)$ measures are different. The shape on the right is a thin circular ring whose computed $\mathcal{E}_{avg}(S)$ measure is very small (in this particular case it is 0.0524). This is as expected because such a circular ring has a small ellipticity measure $\mathcal{E}_\rho(S)$, for all $\rho \in (0, 1]$.

The graphs of the average ellipticities $\mathcal{E}_{(0,t]}(S)$, for $t \in (0, 1]$ are displayed in the third row. As it can be seen the shape of these graphs vary. Indeed, some of them are monotonic while the others have clearly identified picks. Thus, even such specific intervals provide a diversity of $\mathcal{E}_{(a,b]}(S)$ measures. Of course, the introducing the whole family of intervals $(a, b]$ (with $0 < a < b \le 1$) would increase such a diversity, in both terms: **(a)** the shape of the graph of $\mathcal{E}_{(a,b]}(S)$; and **(b)** the value range of $\mathcal{E}_{(a,b]}(S)$. Three randomly selected shapes, and their corresponding graphs $\mathcal{E}_{(a,b]}(S)$, are dis-

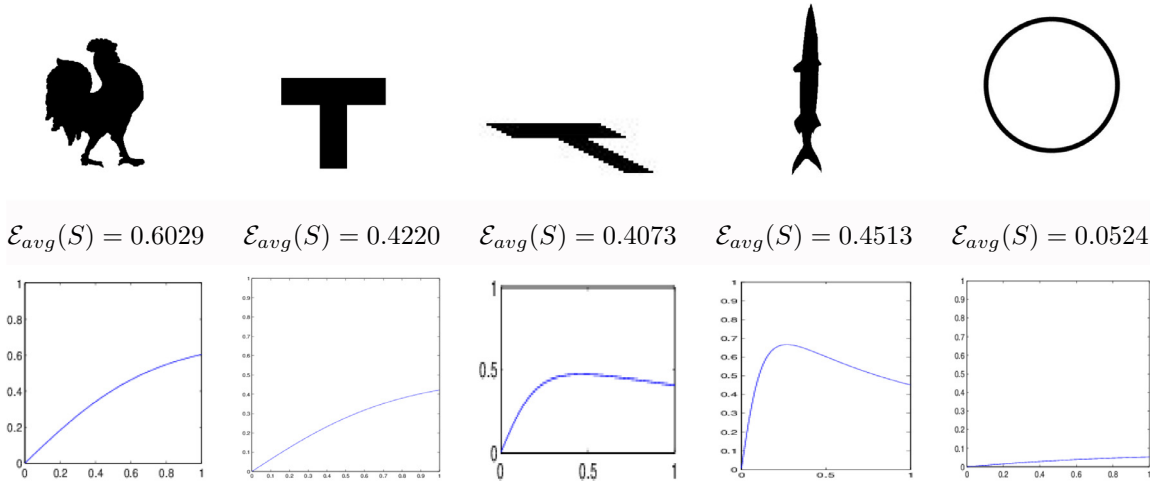

Fig. 4. Randomly selected shapes (top row) and their corresponding average ellipticities $\mathcal{E}_{avg}(S)$ (second row). The graphs of $\mathcal{E}_{(0,t]}(S)$, while t ranges over (0, 1] are in the third row.

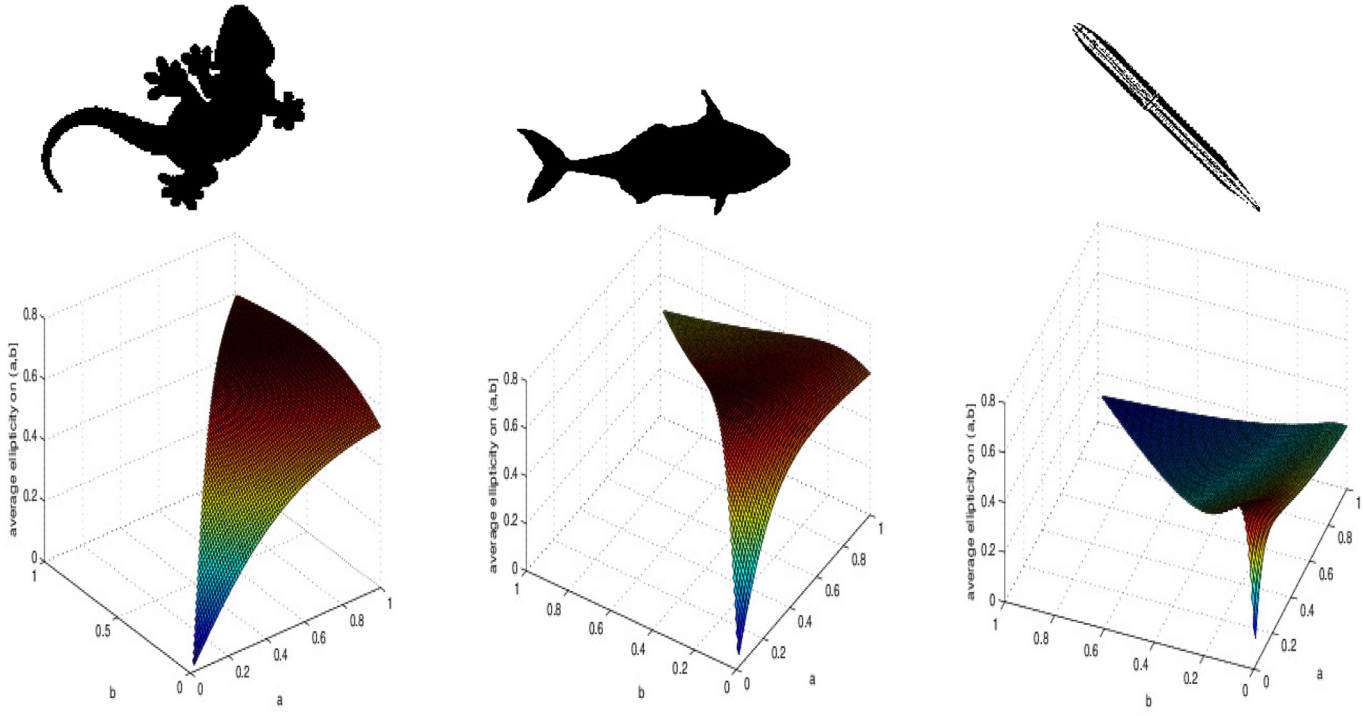

Fig. 5. Randomly selected shapes and their corresponding average ellipticity graphs $\mathcal{E}_{(a,b]}(S)$, with $0 < a < b \leq 1$.

played in Fig. 5, just for an illustration. Variance in both senses, as given in **(a)** and **(b)**, is obvious.

3.3. Relation with some of the known results

Results derived here strongly relate to some of the well known results. The relationship with the circularity measure, from [33], has already been explained in Corollary 1. Here are two more notes explaining relationships with the results that have been in a frequent use in image processing and computer vision tasks [25]. The first note relates to a question: *Which ellipse best fits to a given shape?* The answer which comes out from this paper is in accordance with a popular choice, used intensively in the past, as discussed in Note 1.

Note 1. The quantities $\sqrt{\mathcal{H}_1(S) - \sqrt{\mathcal{H}_2(S)}}$ and $\sqrt{\mathcal{H}_1(S) + \sqrt{\mathcal{H}_2(S)}}$ are axes of the ellipse which is very often used to approximate the planar regions [25]. Thus, we can say that the results of the Lemma 3 are in accordance with this standard method. Indeed, the ellipse $E(\rho)$, having the axes length ratio as in (16), if compared with the shape S leads to the maximal computed ellipticity, $\mathcal{E}_{\max}(S)$, as stated by Lemma 3. This gives an additional argument to use this ellipse as an approximation of the shape S, as it has been used in the past – of course, supported by different arguments. □

The next note relates to a very popular [6,24] affine invariant $\mathcal{P}(S) = m_{2,0}(S) \cdot m_{0,2}(S) - m_{1,1}(S)^2$. Another way to interpret the meaning of $\mathcal{P}(S)$ is a *geometric interpretation* given in [31] and the *shape interpretation* of $\mathcal{P}(S)$ explained recently in [34]. Thus, here we establish a new interpretation of $\mathcal{P}(S)$ and show that it can be observed as a result of a comparison of the shape S with a 'best fit' ellipse.

Note 2. The expressions of $\mathcal{H}_1(S)$ and $\mathcal{H}_2(S)$), as in (4), give

$$\mathcal{H}_1(S)^2 - \mathcal{H}_2(S)) \;=\; 4\cdot m_{2,0}(S)\cdot m_{0,2}(S) - 4\cdot m_{1,1}(S)^2, \tag{25}$$

which leads to an alternative expression for the maximal shape ellipticity $\mathcal{E}_{\max}(S)$:

$$\max_{\rho\in(0,1]} \mathcal{E}_\rho(S) = \frac{1}{2\cdot\pi\cdot\sqrt{\mathcal{H}_1(S)^2 - \mathcal{H}_2(S)}} = \frac{1}{4\cdot\pi\cdot\sqrt{m_{2,0}(S)\cdot m_{0,2}(S) - m_{1,1}(S)^2}}. \tag{26}$$

As it has been mentioned, the quantity

$$\mathcal{P}(S) = m_{2,0}(S)\cdot m_{0,2}(S) - m_{1,1}(S)^2 \tag{27}$$

is the well-known afine invariant [6,24,32] and has already been used to measure the shape ellipticity [24,34]. The ellipticity measure $\mathcal{E}_R(S)$ defined in [24] and simplified in [34] is

$$\mathcal{E}_R(S) \;=\; \frac{1}{16\cdot\pi^2\cdot\mathcal{P}(S)}. \tag{28}$$

Thus, the following identity

$$\mathcal{E}_{max}(S) \;=\; \max_{\rho\in(0,1]} \mathcal{E}_\rho(S) \;=\; \sqrt{\mathcal{E}_R(S)} \;=\; \frac{1}{4\cdot\pi\cdot\sqrt{\mathcal{P}(S)}} \tag{29}$$

is true and shows how another well known result, from the literature, relates to a particular ellipticity measure considered in this paper. □

4. Concluding remarks

In this paper we put under the same umbrella several well known results which treat the shape ellipticity issues. Actually, the initial motivation for our work was to find a more efficient way for the computation of the ellipticity measures from the family $\{\mathcal{E}_\rho(S) \mid 0 < \rho \le 1\}$, introduced recently [1]. The measures from the family show the degree to which a given shape looks like an ellipse with a given ratio between its axes length. As such, they have a predictable behavior, contrary to generic measures. We have succeed and find a closed and explicit formula for such a computation. The new formula enables a fast and straightforward computation of all the ellipticity measures $\mathcal{E}_\rho(S)$. It replaces the previous formula, which has required an optimization procedure.

Exploiting the new formula, which also enables an easy manipulation and analysis of the properties of $\mathcal{E}_\rho(S)$ measures, we found much more. We have discovered some of the shape features which have not been considered in the literature so far. In particular, we have defined the maximum shape ellipticity measure and an infinite family of the average shape ellipticity measures. In addition, it has been shown that some of the well known results are in a strong relation with the results obtained in this paper. More precisely, the following has been shown:

- the circularity measure from [33] coincides with the measure $\mathcal{E}_{\rho=1}(S)$;
- the ellipticity measure $\mathcal{E}_R(S)$, introduced in [24], coincides with the squared value of the maximal shape ellipticity measure $\mathcal{E}_\rho(S)$ – i.e. $\mathcal{E}_R(S) = \left(\max_{\rho\in(0,1]}\{\mathcal{E}_\rho(S)\}\right)^2$;
- A new insight on the famous second order afine moment invariant $\mathcal{P}(S)$ [6] has been given;
- It has turned out that the ellipse $E(\rho)$ which fits best with a given shape coincides with the ellipse commonly used in the literature for a long time, but derived under another arguments.

All statements are given with strict mathematical proofs. Theoretical observations are accompanied with illustrative examples, given to support a better understanding of the results established.

Acknowledgments

The authors gratefully acknowledge support from the Singapore Ministry of Education through grant MOE2013-T2-1-010, and from the Serbian Ministry of Education, Science, and Technology.

Appendix

Proof of Lemma 1. Every point (x, y) in the rotated shape $S(\alpha)$ corresponds to a point $(x\cdot\cos\alpha - y\cdot\sin\alpha,\; x\cdot\sin\alpha + y\cdot\cos\alpha)$ in the shape S, taken in its original position. Thus,

$$\int\int_{S(\alpha)} \left(\frac{x^2}{\rho} + \rho\cdot y^2\right)dxdy \tag{30}$$

$$= \cos^2\alpha\cdot\left(\frac{1}{\rho}\cdot m_{2,0}(S) + \rho\cdot m_{0,2}(S)\right) + \sin(2\alpha) \cdot\left(\rho\cdot m_{1,1}(S) - \frac{1}{\rho}\cdot m_{1,1}(S)\right) + \sin^2\alpha\cdot\left(\frac{1}{\rho}\cdot m_{0,2}(S) + \rho\cdot m_{2,0}(S)\right) \tag{31}$$

$$= \cos(2\alpha)\cdot\frac{m_{2,0}(S) - m_{0,2}(S)}{2}\cdot\left(\frac{1}{\rho} - \rho\right) + \sin(2\alpha)\cdot m_{1,1}(S)\cdot\left(\rho - \frac{1}{\rho}\right) + \frac{m_{2,0}(S) + m_{0,2}(S)}{2}\cdot\left(\frac{1}{\rho} + \rho\right). \tag{32}$$

So, we have shown that

$$\int\int_{S(\alpha)} \left(\frac{x^2}{\rho} + \rho\cdot y^2\right)dxdy \;=\; A\cdot\cos(2\alpha) + B\cdot\sin(2\alpha) + C$$

where A, B, and C do not depend on α. Since an elementary calculus says

$$\min_{\alpha\in[0,\pi)}\{A\cdot\cos(2\alpha) + B\cdot\sin(2\alpha) + C\} = C - \sqrt{A^2 + B^2}$$

we deduce the following equality which establishes the proof:

$$\min_{\omega\in[0,2\pi]}\{\int\int_{S(\omega)} \left(\tfrac{x^2}{\rho} + \rho\cdot y^2\right) \quad dx \quad dy\} \;=\; \tfrac{\rho^2+1}{2\cdot\rho}\cdot\mathcal{H}_1(S) - \tfrac{1-\rho^2}{2\cdot\rho}\cdot\sqrt{\mathcal{H}_2(S)}.$$ □

References

[1] M.A. Aktaş, J. Žunić, A family of shape ellipticity measures for galaxy classification, SIAM J. Imaging Sci. 6 (2013) 765–781.
[2] O. Arandjelović, Computationally efficient application of the generic shape illumination invariant to face recognition from video, Pattern Recognit. 45 (2012) 92–103.
[3] J. Cates, P.T. Fletcher, M. Styner, M. Shenton, R. Whitaker, Shape modeling and analysis with entropy-based particle systems, in: Proc. Information Processing in Medical Imaging (IPMI), Lecture Notes in Computer Science, volume 4584, 2007, pp. 333–345.
[4] T. Cootes, C. Taylor, D. Cooper, J. Graham, Active shape models – their training and application, Comput. Vision Image Understanding 61 (1995) 38–59.
[5] A.-N. Denga, C.-H. Weia, C.-Y. Gwoa, Stable, fast computation of high-order Zernike moments using a recursive method, Pattern Recognit. 56 (2016) 16–25.
[6] J. Flusser, T. Suk, Pattern recognition by affine moment invariants, Pattern Recognit. 26 (1993) 167–174.
[7] Z. Frei, P. Guhathakurta, J.E. Gunn, J.A. Tyson, A catalog of digital images of 113 nearby galaxies, Astron. J. 111 (1996) 174–181.
[8] A.V. Gaikwad, S.J. Shigwan, S.P. Awate, A statistical model for smooth shapes in Kendall shape space, in: Proc. Medical Image Computing and Computer-Assisted Intervention (MICCAI), Lecture Notes in Computer Science, volume 9351, 2015, pp. 628–635.
[9] T. Gautama, D.P. Mandić, M.M. Van Hulle, Signal nonlinearity in fMRI: a comparison between BOLD and MION, IEEE Trans. Med. Images 22 (2003) 636–644.
[10] E. Grisan, M. Foracchia, A. Ruggeri, A novel method for the automatic grading of retinal vessel tortuosity, IEEE Trans. Med. Imaging 27 (2008) 310–319.
[11] M. Hu, Visual pattern recognition by moment invariants, IRE Trans. Inf. Theory 8 (1962) 179–187.

[12] F. Janan, M. Brady, Shape description and matching using integral invariants on eccentricity transformed images, Int. J. Comput. Vision 113 (2015) 92–112.
[13] B. Joachimi, E. Semboloni, P.E. Bett, J. Hartlap, S. Hilbert, H. Hoekstra, P. Schneider, T. Schrabback, Intrinsic galaxy shapes and alignments I. Measuring and modelling COSMOS intrinsic galaxy ellipticities, Mon. Not. R. Astron. Soc. 431 (2013) 477–492.
[14] L. Kopanja, D. Žunić, B.B. Lončar, G. Saso, M.M. Tadić, Quantifying shapes of nanoparticles using modified circularity and ellipticity measures, Measurement 92 (2016) 252–263.
[15] J. Krúger, J. Ehrhardt, H. Handels, Statistical appearance models based on probabilistic correspondences, Med. Image Anal. 37 (2017) 146–159.
[16] K. Krzysztof Misztal, J. Tabor, Ellipticity and circularity measuring via Kullback–Leibler divergence, J. Math. Imaging Vision 55 (2016) 136–150.
[17] D.R. Lee, T. Sallee, A method of measuring shape, Geog. Rev. 60 (1970) 555–563.
[18] S. Lekshmi, K. Revathy, S.R. Prabhakaran Nayar, Galaxy classification using fractal signature, Astron. Astrophys. 405 (2003) 1163–1167.
[19] Y.-B. Lin, C.-P. Young, High-precision bicycle detection on single side-view image based on the geometric relationship, Pattern Recognit. 63 (2017) 334–354.
[20] N. Otsu, A threshold selection method from gray level histograms, IEEE Trans. Syst. Man Cybern. 9 (1979) 62–66.
[21] P.M. Merkel, B.M. Schäfer, A theoretical estimate of intrinsic ellipticity bispectra induced by angular momenta alignments, Mon. Not. R. Astron. Soc. 445 (2014) 2918–2929.
[22] D. Proffitt, The measurement of circularity and ellipticity on a digital grid, Pattern Recognit. 15 (1982) 383–387.
[23] E. Rahtu, M. Salo, J. Heikkilä, A new convexity measure based on a probabilistic interpretation of images, IEEE Trans. Pattern Anal. Mach. Intell. 28 (2006) 1501–1512.
[24] P.L. Rosin, Measuring shape: ellipticity, rectangularity, and triangularity, Mach. Vision Appl. 14 (2003) 172–184.
[25] M. Sonka, V. Hlavac, R. Boyle, Image Processing, Analysis, and Machine Vision, PWS, 1998.
[26] M. Stojmenović, A. Nayak, J. Žunić, Measuring linearity of planar point sets, Pattern Recognit. 41 (2008) 2503–2511.
[27] A.Q. Tool, A method for measuring ellipticity and the determination of optical constants of metals, Phys. Rev. (Ser. I) 31 (1910) 1–25.
[28] M. Vaillant, J. Glaunès, Surface matching via currents, in: Proc. Information Processing in Medical Imaging (IPMI), Lecture Notes in Computer Science, volume 3565, 2005, pp. 381–392.
[29] B. Wang, Shape retrieval using combined Fourier features, Opt. Commun. 284 (2011) 3504–3508.
[30] X. Wang, T. Yang, F. Guo, Image analysis by circularly semi-orthogonal moments, Pattern Recognit. 49 (2016) 226–236.
[31] D. Xu, H. Li, Geometric moment invariants, Pattern Recognit. 41 (2008) 240–249.
[32] D. Žunić, J. Žunić, Shape ellipticity from Hu moment invariants, Appl. Math. Comput. 226 (2014) 406–414.
[33] J. Žunić, K. Hirota, P.L. Rosin, A Hu moment invariant as a shape circularity measure, Pattern Recognit. 43 (2010) 47–57.
[34] J. Žunić, D. Žunić, Shape interpretation of the second moment invariants, J. Math. Imaging Vision 56 (2016) 125–136.

Joviša Žunić is with the Mathematical Institute of the Serbian Academy of Sciences and Arts. His research interests include: image processing and computer vision, digital image analysis, digital geometry, shape representation and coding of digital objects, discrete mathematics, combinatorial optimization, neural networks and number theory.

Ramakrishna Kakarala has worked in both academia and industry; prior to joining NTU, he spent 8 years at Agilent Laboratories in Palo Alto, and at Avago Technologies in San Jose. He received the Ph.D. in Mathematics at UC Irvine, after completing a B.Sc. in Computer Engineering at the University of Michigan.

Mehmet Ali Aktas obtained his bachelor degree in Computer Engineering from Girne American University in 2006, and M.Sc. in Artificial Intelligence from University of Exeter, Exeter, in 2009. He stayed on in Exeter and completed his Ph.D. in 2012 with a dissertation on the "Shape Descriptors". Now, he is working at Toros University as an Asst. Prof. in Computer Engineering department. His researches include: image processing, shape analysis, shape classification and pattern recognition.